PLANCK CLUSTER PAPER

SB[1], JPH[1], FM, PD[1]

Draft Version March 23, 2018

ABSTRACT

We propose to continue our program of optical imaging to unveil all of the most massive clusters in the observable Universe. We start from the all-sky Planck Sunyaev-Zeldovich (SZ) catalogs, which contain several hundred high significance (signal-to-noise ratio, SNR > 5) unconfirmed cluster candidates. Since SZ selection favors high mass clusters and the Planck confirmation process favored low redshift systems, the highest significance unconfirmed candidates are, therefore, likely massive clusters ($M_{500} > 5 \times 10^{14}$ M$_\odot$) at relatively high redshift ($z > 0.5$). Our proposed observations, using MOSAIC-3 on Mayall, are designed to confirm the presence of a brightest cluster galaxy (to $z \sim 1$) and red sequence of accompanying cluster members (to $z \sim 0.7$). Preliminary results from our observations over the past two years have validated our approach by the detection of optical clusters in a number of Planck candidates, including the discovery of rich systems at $z = 0.553$ and $z = 0.830$ that rival the most massive clusters known. The proposed observations represent the first step required to provide a complete all-sky census throughout the observable Universe of the most massive, high redshift clusters. Their expected high redshift and high mass make the unconfirmed Planck clusters, arguably, the most important available sample for probing deviations from ΛCDM and defining the high-mass end of the cluster mass function.

Subject headings:

1. INTRODUCTION

this section has not been edited and is just a bunch of stuff copy and pasted. I did update some of the references. Massive galaxy clusters at high redshifts are rare beasts that hold important clues to the evolution of structure in the Universe and in principle can help probe (or falsify) structure formation models under the ΛCDM paradigm (e.g., Mortonson et al. 2011; Harrison & Coles 2012; Harrison & Hotchkiss 2012; Waizmann et al. 2012; Zitrin et al. 2009). Galaxy clusters also harbor a significant fraction of the visible baryons in the Universe, in the form of a hot intracluster medium that leaves an imprint on the Cosmic Microwave Background (CMB) though the Sunyaev-Zel'dovich (SZ; Sunyaev & Zeldovich 1972 effect.

The surface brightness of the SZ effect does not depend on redshift, therefore providing uniform samples of massive clusters up to arbitrary distances. This has been borne out by the large area surveys of the Atacama Cosmology Telescope (ACT; Swetz et al. 2011) and the South Pole Telescope (SPT; Carlstrom et al. 2011 that have detected hundreds of massive clusters since 2008 up to redshifts of $z \sim 1.4$ (see Reichardt et al. 2013 and Hasselfield et al. 2013 for latest results). Now, Planck has released an all-sky SZ sample (PSZ; Planck Collaboration et al. 2014) that contains 861 confirmed clusters (of which most [683] were known previously) and another 366 unconfirmed cluster candidates.

We led the ACT cluster confirmation process using 4-m class telescopes; now we propose to use our well-established expertise to identify Planck clusters. The recent SZ cluster samples have opened a new window into extreme systems, the most massive clusters at high redshift (Foley et al. 2011; Menanteau et al. 2012), prompt-

ing studies that match their observed numbers with the abundance predictions of ΛCDM cosmology (Hoyle et al. 2011, Mortonson et al. 2011, Waizmann et al. 2012). There are few, if any, clusters at high redshift ($z > 0.8$) and high mass ($M_{200} > 10^{15}$ M$_\odot$) in the cosmological simulations (see Tinker et al. 2008), so the halo mass function at high-z and high-M is essentially unconstrained. Thus, with the proposed observations we will determine the abundance of massive clusters at high redshift making a direct observational measurement of the high-z, high-M end of the halo mass function. For example, one of the most impressive results of the ACT SZ survey is our discovery of the high redshift ($z = 0.87$), extreme cluster "El Gordo" (ACT-CL J0102-4915), the most significant SZ detection of the whole survey (and also of the SPT survey). Our recent HST weak-lensing analysis has provided an independent mass estimation $M_{200a} = (3.1 \pm 0.7) \times 10^{15}$ M$_\odot$ (Jee et al. 2013) that confirms our earlier mass estimates for the cluster (Menanteau et al. 2012). Based on its estimated mass alone, "El Gordo" is a very rare system within the ACT+SPT (2800 sq. deg.) survey area, but is still consistent with the expectations of ΛCDM. We are now at a unique moment in cluster science where we can discover all massive clusters in the observable universe. This census will measure the high-mass, high-redshift cluster mass function, and determine the extent of deviations from the theoretical halo mass function (Jenkins et al. 2001; Tinker et al. 2008).

Assuming WMAP7 cosmology (Komatsu et al. 2011) with the Tinker et al. (2008) halo mass function, there should be only ~ 4 clusters as massive as El Gordo ($\leq 2 \times 10^{15}$ M$_\odot$) at $z > 0.6$ in the full area covered by the Planck PSZ catalog (83.7% of the sky). Although Plancks larger beam size (compared to both ACT and SPT) makes it more sensitive to clusters at lower red-

[1] Rutgers;boada@physics.tamu.edu

shifts (due to their larger projected area on the sky), among the 861 confirmed clusters in the recently released all-sky Planck SZ catalog are the two highest significance high-redshift SZ detections from ACT (as well as several other ACT and SPT clusters). This confirms the ability of Planck to unambiguously detect the most massive clusters at high redshift. In fact Planck reports "El Gordo" ($z = 0.87$) and ACT-CL J2327.40204 ($z = 0.701$) at S/N values of 8.0 and 6.3, respectively. And as Figure 2 (right panel) shows, these are the two most massive Planck clusters in the confirmed sample at high redshift. For the new clusters we confirm, our experimental design allows us to estimate photometric redshifts, which will be sufficiently accurate for a meaningful estimate of the clusters mass from the Planck SZ signal.

Unless otherwise noted, throughout this paper, we use a concordance cosmological model ($\Omega_\Lambda = 0.7$, $\Omega_m = 0.3$, and $H_0 = 70$ km s^{-1}Mpc^{-1}), assume a Chabrier initial mass function (Chabrier 2003), and use AB magnitudes (Oke 1974).

2. DESIGN

Among the recently released, second, all-sky PSZ catalog[2] (hereafter PSZ2; Planck Collaboration et al. 2016) there are 450 unconfirmed SZ detections with S/N > 4.5. The vast majority of these must lie at high-z because the Planck confirmation process mostly relied on existing catalogs with a preference for low-z clusters. Furthermore, the confirmed sample has a small fraction (3%) of $z > 0.6$ clusters compared to that expected ($\sim 20\%$) based on the theoretical halo mass function (Jenkins et al. 2001; Tinker et al. 2008). If other clusters like "El Gordo" exist, they are hiding as high-significance candidates within the objects in this catalog. The design of the observations is to use both optical and near-infrared (NIR) imaging to confirm the SZ detections as real clusters and provide photometric redshifts using the multi-color information.

Our strategy is to use the Kitt Peak National Observatory (KPNO) Mayall-4m telescope imaging as the first and fundamental step to confirm the highest significance detections in the PSZ2 catalog that are visible across the entire northern sky. Following closely the procedure used for ACT follow-up citation?, targets are prioritized by SZ signal-to-noise (S/N). We choose to initially report on targets with PSZ2 S/N > 5 as the statistical reliability of PSZ2 cluster candidates is quite high: according to the Planck team $\sim 90\%$ of candidates at S/N > 5 turn out to be "real" clusters (citation? maybe show the figure from the proposal).

Optical imaging will be sufficient to confirm nearly all of the candidates, but for the highest redshift ones, NIR data will be necessary. Again following the procedure for ACT cluster follow-up: those candidates with some evidence for a high-z brightest cluster galaxy (BCG; note that we can detect BCGs to $z \sim 1.5$) will be targeted with NIR observations to confirm the presence of a BCG and detect the red sequence of cluster members. Observational priority again is given to higher S/N candidates.

2.1. *Observations*

All observations were conducted with the KPNO Mayall telescope. The optical observations were made with the MOSAIC camera mounted at the prime focus. Two detector packages were used for the observations. The earlier MOSAIC1.1 instrument consisted of eight 2048 × 4096 SITe CCDs, arranged 2 × 4, separated by a ~ 50 pixels gap with a pixel scale of 0.″26 pixel^{-1}. MOSAIC1.1 was replaced with Mosaic3, in year?, and consists of four new 4k×4k, 15 micron pixel, 500-micron thick LBNL deep-depletion CCDs. Because the only change from MOSAIC1.1 to MOSAIC3 are the CCDs and controllers both versions have a $36' \times 36'$ field-of-view.

The near-IR observations utilized the National Optical Astronomy Observatory (NOAO) Extremely Wide-Field Infrared Imager (NEWFIRM; Probst et al. 2004). The instrument consists of four InSb 2048 × 2048 pixel arrays arranged 2 × 2 with approximately 1′ gaps between each of the CCDs. The detector has a plate scale of 0.″4 pixel^{-1} and a $28' \times 28'$ field-of-view.

need to talk about the dithering

The optical observing strategy consists of targeted $griz$ observations of individual candidates with exposure times of 350 s, 350 s, 1100 s and 1100 s (assuming dark conditions) to provide 5σ detections limits of $g = ??$, $r = 24.5$, $i = 24.5$, $z = 24.2$ ensuring the unambiguous detection of the faint (i.e., 0.4L$_\star$) galaxies in the red cluster sequence up to $z \sim 1.0$ (citation?) and of brightest cluster galaxies (BCGs) to higher redshifts. The choice of filters in our program is driven by the need to segregate early-type galaxies in the cluster through their colors (or photometric redshifts) by sampling blueward and red-ward of the 4000Å break. Our depths are quite a bit different that the designed depths. Should we mention that here, or wait till later on when we are discussing how we actually did?

For the NEWFIRM observations, we obtained 3600 s of Ks band imaging using 60 s exposures (5 coadded 12 s exposures) taken at 60 different dither positions distributed quasi-randomly over a square $100'' \times 100''$ region. This produced reduced images with uniform exposure and sky level. The final dithered images cover approximately $28' \times 28'$ which comfortably matches the MOSAIC observations.

A NEWFIRM integration of 3600 s allows us to reach a limiting Ks magnitude of ~ 22.0 (AB, 3σ). This magnitude limit corresponds to $\sim M_\star + 2$ in the cluster luminosity function at $z = 1.0$ as measured by De Propris et al. (1999), and assuming Ks AB = Ks Vega +1.86. This surface brightness limit corresponds to $\sim M_\star + 1.0$ at $z = 1.5$, sufficient for detecting sub L$_\star$ at this limit, allowing for confident detection of the BCG and associated red cluster sequence.

TABLE 1 Basic properties of the galaxy clusters candidates targeted for observation with the MOSAIC and NEWFIRM instruments: Column 1: Cluster name; Column 2: The right ascension of the cluster; Column 3: The declination of the cluster; Column 4: the PSZ1 catalog S/N ratio; Column 5: the PSZ2 catalog S/N ratio; Column 6: The date of MOSAIC observations; Column 6: The data of NEWFIRM observations.

Cluster (1)	RA (J2000) (2)	DEC (J2000) (3)	PSZ1 SNR (4)	PSZ2 SNR (5)	MOSAIC Obs. (6)	NEWFIRM Obs. (7)
PSZ1 031.91+67.94	14:29:02	+24:37:33.38	5.23	nan	Feb, 2014	Feb, 2016
PSZ1 055.83-41.64	21:57:14	-2:31:51	5.72	nan	Oct, 2014	Nov, 2014
PSZ1 084.62-15.86	21:49:44	+33:10:23.81	6.01	nan	Oct, 2014	–
PSZ1 096.44-10.40	22:19:35	+44:31:05.27	6.55	nan	Oct, 2014	Nov, 2014
PSZ1 102.86-31.07	23:33:08	+28:43:51.60	6.12	nan	Oct, 2014	Nov, 2014
PSZ1 102.97-04.77	22:34:47	+52:43:13.90	5.64	nan	Oct, 2014	–
PSZ1 105.91-38.39	23:53:54	+22:34:21.09	7.16	nan	Oct, 2014	Nov, 2014
PSZ1 108.90-52.04	0:16:38	+09:52:49.98	6.89	nan	Jun, 2017	Nov, 2014
PSZ1 118.06+31.10	15:54:34	+84:10:37.49	6.00	nan	Feb, 2014	Mar, 2014
PSZ1 125.54-56.25	0:57:17	+06:35:23.29	4.86	nan	Nov, 2014	–
PSZ1 127.55+20.84	3:10:51	+82:25:43.91	5.91	nan	Oct, 2014	Nov, 2014
PSZ1 138.60-10.85	2:27:02	+49:04:54.07	8.26	nan	Oct, 2014	Nov, 2014
PSZ1 142.17+37.28	9:18:56	+70:52:01.14	5.79	nan	Feb, 2014	Mar, 2014
PSZ1 142.38+22.82	6:13:40	+71:52:21.02	5.82	nan	Feb, 2014	Mar, 2014
PSZ1 146.00-49.42	1:51:35	+10:44:02.79	6.62	nan	Oct, 2014	Nov, 2014
PSZ1 148.20+23.49	6:37:46	+66:54:24.40	8.40	nan	Feb, 2014	Mar, 2014
PSZ1 153.41+36.58	8:42:40	+62:34:31.61	6.85	nan	Feb, 2014	Mar, 2014
PSZ1 153.56+36.23	8:39:31	+62:31:30.58	5.96	nan	Feb, 2014	Mar, 2014
PSZ1 162.30-26.92	3:24:26	+24:00:44.46	6.56	nan	Oct, 2014	Nov, 2014
PSZ1 169.80+26.10	7:30:08	+48:20:02.06	5.32	nan	Oct, 2014	–
PSZ1 182.49-57.09	2:44:20	-7:55:37	5.09	nan	Nov, 2014	–
PSZ1 183.26+12.25	6:42:56	+31:49:07.58	5.43	nan	Oct, 2014	–
PSZ1 185.93-31.21	4:11:39	+06:16:00.67	5.90	nan	Jan, 2014	Nov, 2014
PSZ1 206.45+13.89	7:29:59	+11:56:22.64	5.90	nan	Feb, 2014	Mar, 2014
PSZ1 224.82+13.62	8:01:42	-4:03:54	5.51	nan	Jan, 2014	–
PSZ1 244.48+34.06	9:49:52	-7:29:28	8.14	nan	Jan, 2014	Mar, 2014
PSZ1 249.01+73.75	11:56:46	+16:55:43.68	7.14	nan	Feb, 2014	Mar, 2014
PSZ1 286.25+62.68	12:21:10	+00:47:34.05	5.52	nan	Feb, 2014	Feb, 2016
PSZ1 341.69+50.66	14:25:20	-4:59:54	5.48	nan	Feb, 2014	–
PSZ2 022.03+17.75	17:28:37	-1:13:03	5.64	6.20	Jun, 2017	Feb, 2016
PSZ2 023.05+20.52	17:20:47	+00:58:06.58	nan	5.57	Jun, 2017	–
PSZ2 024.46-18.08	19:42:23	-15:26:09	nan	6.98	Jun, 2017	–
PSZ2 027.77+10.88	18:03:22	+00:25:57.59	nan	6.42	Jun, 2016	–
PSZ2 028.15-08.62	19:13:41	-8:08:26	5.07	7.67	Jun, 2017	–
PSZ2 029.66-47.63	21:45:44	-21:46:49	nan	5.74	Nov, 2016	–
PSZ2 029.80-17.40	19:48:32	-10:31:40	6.59	9.01	Jun, 2016	–
PSZ2 031.41-19.16	19:57:41	-9:53:56	4.60	5.69	Jun, 2017	–
PSZ2 032.12-14.96	19:43:34	-7:27:45	8.21	9.12	Jun, 2017	Nov, 2016
PSZ2 033.27-17.54	19:54:52	-7:36:11	5.78	6.86	Jun, 2017	–
PSZ2 036.69-15.67	19:54:05	-3:50:23	nan	5.69	Jun, 2017	–
PSZ2 043.44-41.27	21:36:44	-10:17:48	nan	5.55	Jun, 2017	–
PSZ2 044.83+10.02	18:36:39	+15:04:49.72	7.27	9.27	Oct, 2015	Feb, 2016
PSZ2 045.50-08.62	19:45:25	+07:04:29.08	4.57	5.63	Jun, 2017	–
PSZ2 047.53+08.55	18:46:59	+16:50:35.39	5.82	6.55	Jun, 2016	–
PSZ2 048.47+34.86	17:02:08	+27:08:48.05	nan	5.74	Jun, 2016	Feb, 2016
PSZ2 065.35-08.01	20:26:04	+24:08:06.72	nan	5.83	Jun, 2016	–
PSZ2 071.67-42.76	22:30:54	+05:42:05.22	8.82	8.63	Oct, 2014	Nov, 2014
PSZ2 075.08+19.83	18:46:48	+45:46:33.27	nan	5.74	Jun, 2016	–
PSZ2 089.06-11.79	21:52:53	+39:03:52.50	nan	5.72	Nov, 2016	–
PSZ2 092.11-33.73	23:01:37	+22:28:59.71	nan	5.81	Nov, 2016	Nov, 2016
PSZ2 092.46-35.22	23:05:50	+21:19:27.96	5.47	6.73	Oct, 2014	Nov, 2014
PSZ2 093.04-32.38	23:01:43	+24:02:24.90	5.69	6.03	Oct, 2014	Nov, 2014
PSZ2 096.43-20.89	22:48:09	+35:33:21.47	nan	5.81	Jun, 2016	Nov, 2016
PSZ2 098.38+77.22	13:18:25	+38:35:06.94	4.71	5.51	Jun, 2017	Nov, 2016
PSZ2 100.22+33.81	17:13:41	+69:22:24.33	nan	5.69	Jun, 2017	–
PSZ2 100.45+16.79	20:18:34	+66:47:07.85	nan	11.79	Oct, 2015	Nov, 2015
PSZ2 104.15-38.85	23:48:48	+21:43:24.60	nan	6.41	Jun, 2016	Nov, 2016
PSZ2 106.11+24.11	19:21:24	+74:33:21.87	nan	5.70	Jun, 2017	–
PSZ2 107.41-09.57	23:13:47	+50:19:32.01	nan	10.69	Jun, 2016	Nov, 2015
PSZ2 107.83-45.45	0:07:35	+16:07:51.05	nan	7.09	Nov, 2016	Nov, 2016
PSZ2 112.07-39.86	0:15:30	+22:14:43.50	nan	5.72	Nov, 2016	Nov, 2016
PSZ2 120.76+44.14	13:12:39	+72:53:23.47	nan	5.59	Jun, 2017	Feb, 2016
PSZ2 123.35+25.39	1:41:20	+88:13:14.57	5.90	10.86	Oct, 2014	Feb, 2016
PSZ2 123.84+25.75	2:55:30	+88:24:01.91	5.04	5.81	Nov, 2016	Feb, 2016
PSZ2 125.55+32.72	11:25:35	+83:57:29.12	nan	6.49	Nov, 2016	Feb, 2016
PSZ2 127.35-10.69	1:19:42	+51:56:15.39	5.58	6.94	Oct, 2014	Nov, 2014
PSZ2 136.31+54.67	11:47:50	+60:45:56.07	nan	6.92	Jun, 2017	Feb, 2016
PSZ2 137.24+53.93	11:41:07	+61:11:39.02	nan	7.87	Nov, 2016	Feb, 2016
PSZ2 137.58+53.88	11:39:27	+61:09:01.04	5.73	8.18	Feb, 2014	Mar, 2014
PSZ2 145.25+50.84	10:53:26	+60:51:43.24	nan	5.98	Jun, 2017	Feb, 2016
PSZ2 146.88+17.13	5:34:10	+65:43:14.28	nan	6.13	Nov, 2016	Feb, 2016
PSZ2 153.56+36.82	8:44:32	+62:24:41.96	nan	15.90	Nov, 2016	Nov, 2015

TABLE 1 Continued

Cluster	RA (J2000)	DEC (J2000)	PSZ1 SNR	PSZ2 SNR	MOSAIC Obs.	NEWFIRM Obs.
(1)	(2)	(3)	(4)	(5)	(6)	(7)
PSZ2 153.68+36.96	8:45:33	+62:17:12.13	nan	5.07	Nov, 2016	Nov, 2015
PSZ2 163.22-26.48	3:28:29	+23:50:15.15	nan	6.35	Nov, 2016	Feb, 2016
PSZ2 165.39+09.22	5:47:59	+46:08:39.24	nan	5.60	Nov, 2016	Nov, 2016
PSZ2 166.27-24.71	3:42:39	+23:24:41.39	nan	9.58	Nov, 2016	Nov, 2015
PSZ2 166.27-25.02	3:41:44	+23:11:00.45	nan	8.09	Nov, 2016	Nov, 2016
PSZ2 167.44-38.06	3:09:12	+12:37:11.49	6.11	7.66	Oct, 2014	–
PSZ2 171.79-42.08	3:08:40	+07:24:32.96	nan	5.84	Nov, 2016	Feb, 2016
PSZ2 173.76+22.92	7:17:28	+44:03:27.62	nan	5.80	Nov, 2016	Feb, 2016
PSZ2 181.88-30.77	4:04:21	+09:16:14.87	nan	9.29	Nov, 2016	Nov, 2015
PSZ2 185.45-32.01	4:08:04	+06:06:33.99	6.15	4.99	Jan, 2014	Nov, 2014
PSZ2 189.79-37.25	3:59:37	+00:07:54.80	6.99	7.28	Oct, 2014	Nov, 2014
PSZ2 191.82-26.64	4:38:37	+04:42:02.64	4.76	6.17	Nov, 2016	Feb, 2016
PSZ2 192.40-67.89	2:18:20	-17:45:23	nan	7.03	Nov, 2016	Feb, 2017
PSZ2 194.68-49.76	3:25:22	-9:40:50	5.00	5.71	Nov, 2016	Nov, 2016
PSZ2 210.37-37.00	4:32:44	-14:03:01	nan	9.84	Nov, 2016	Nov, 2015
PSZ2 210.71+63.08	10:51:42	+24:58:09.19	nan	7.37	Jun, 2017	Feb, 2016
PSZ2 210.78-36.25	4:36:07	-14:02:58	nan	6.32	Nov, 2016	Feb, 2016
PSZ2 252.45+73.44	11:58:35	+16:00:18.38	nan	5.57	Jun, 2017	Feb, 2016
PSZ2 305.76+44.79	12:59:54	-18:01:59	4.72	5.72	Jun, 2017	Feb, 2016
PSZ2 310.81+83.91	12:55:01	+21:05:41.16	nan	8.29	Nov, 2016	Feb, 2016
PSZ2 318.46+83.79	12:58:33	+21:08:11.93	6.93	9.40	Feb, 2014	Mar, 2014
PSZ2 320.94+83.69	12:59:47	+21:06:56.63	nan	7.32	Jun, 2017	Feb, 2016
PSZ2 328.96+71.97	13:23:13	+10:43:41.59	nan	5.85	Jun, 2017	Feb, 2016

A summary of our observations is given in Table 1.

3. DATA REDUCTION AND CALIBRATION

Standard image reductions including subtraction of dark frames, flat fielding, sky-subtraction, and bad pixel masking was performed by the NOAO virtual observatory using the MOSAIC (Valdes & Swaters 2007) and NEWFIRM (Swaters et al. 2009) science pipelines. The resultant FITS files consist of fully reduced images with either all single exposure CCDs mosaicked into a single image extension (as in the case of Mosaic1.1 and NEW-FIRM) or as a multi-extension FITS file with each single exposure CCD occupying a separate extension.

We then mosaic each separate exposure into a master mosaic as described in the following section.

3.1. Mosaicking

Combined mosaics are created with SWARP (Bertin et al. 2002). We create three distinct types of mosaics. The individual dither frames are stacked and then median combined to produce the final completed science mosaic. A "detection" is created by combining select science mosaics into a chi2 image using either the i-band and Ks-band or $i-$ and z-band when Ks imaging is not available. Finally we create a set of mosaics use to produce the three color image used for cluster detection. For this we median combine the $griz$ and Ks science mosaics into a "blue" (gr-bands), "green" ($iz-bands$), and "red" (Ks-band) mosaic. All final mosaics have a pixelscale of $0\rlap{.}''25$/pix. The final exposure time is calculated as the median exposure time of the combined images, and similarly the final airmass is median of the individual air masses. need to talk about the weight images

The full parameter file used while creating the mosaics is given in Appendix ??.

3.2. Astrometric Calibration

Each of the final science mosaics produced in the previous section are first astrometrically aligned with *Gaia* (Gaia Collaboration et al. 2016a) Data Release 1 (Gaia Collaboration et al. 2016b) using SCAMP (Bertin 2006) as a part of PHOTOMETRYPIPELINE[3] (PP; Mommert & M. 2017).

Sources are extracted from the mosaics with a signal-to-noise ratio (SNR) of at least ten and with a minimum area of at least 12 pixels. The extracted sources are then matched to the *Gaia* data and a new astrometric solution is calculated. Because the initial astrometric solution from the VO is quite accurate, the resultant corrections are much less than $1''$.

3.3. Photometric Calibration

After the mosaics have been astrometrically aligned, we use PP to produce a photometric solution. PP calculates a photometric zero-point in each of our observed bands by comparing field stars located throughout the mosaic to known photometry from large-area sky surveys. Because our sources are spread across the entire northern sky, and because we prefer to minimize the number of differences between photometric solutions we are limited to two optical surveys and a single IR survey. For the optical data, we first seek photometric data from the *Sloan Digital Sky Survey* (SDSS; York et al. 2000) Data Release 13 (Alam et al. 2015) get a new citation for dr13 this is for dr12. When our target does not lie within the SDSS footprint we utilize the Panoramic Survey Telescope and Rapid Response System (Pan-STARRS; Chambers et al. 2016) Data Release 1 (hereafter PS1; Flewelling et al. 2016). Both surveys provide accurate $griz$ magnitudes and large on-line queriable databases for rapid automated calibration. For our IR imaging, we rely on the *Two Micron All Sky Survey* (2MASS; Skrutskie et al. 2006).

Sources are extracted from the combined mosaics with either a $3''$ or $8''$ diameter aperture for optical and IR sources respectively; sources with a SNR$\geq$ 10 are matched to a survey catalog and a photometric zero-point is determined. We use half of the available stars (with accurate catalog photometry) to derive the zero-

[3] https://github.com/mommermi/photometrypipeline

point resulting in zero-points calculated from approximately $10 - 500$ stars and with typical uncertainties of give zp errors in the different bands.

Should we talk about the difference between us and SDSS? If so, how should we "sum up" the differences in a simple way?

4. ANALYSIS

Lorem ipsum dolor amet swag copper mug meh tilde, put a bird on it live-edge tattooed kinfolk before they sold out locavore selvage leggings raclette literally bicycle rights. Hot chicken kickstarter mustache vinyl roof party. Wayfarers brooklyn truffaut twee umami, venmo irony. Typewriter viral pop-up, listicle vaporware organic af salvia keytar twee chillwave austin +1 offal blog. La croix dreamcatcher snackwave, try-hard intelligentsia taxidermy messenger bag air plant godard mustache celiac glossier echo park. Photo booth readymade authentic glossier biodiesel snackwave beard hammock sriracha before they sold out edison bulb fixie PBR&B. Man bun pabst kogi, crucifix subway tile af tacos cray tumeric lyft cronut lomo tattooed.

4.1. *Source Extraction and Photometry*

For source extraction and photometry estimation we use Source Extractor (hereafter SExtractor; version 2.19.5; Bertin & Arnouts 1996) run dual image mode with the CHI2 detection image as the detection image. See Section 3.1. See Appendix **??** for a complete parameter listing.

4.2. *Photometric Redshifts*

We determine photometric redshifts (photo-z) from the five-band optical and IR (when available) images using Bayesian Photometric Redshifts (BPZ; Benitez 2000; Coe et al. 2006) following the same procedure as in Menanteau et al. (2009).

We assess the effectiveness of our photo-z estimates by comparing with the available spectroscopic redshifts (spec-z) from the SDSS. We use three diagnostics to gauge photo-z accuracy. First, we report the full scatter between the photo-z and spec-z, defined as:

$$\sigma_f = \mathrm{RMS}[\delta z/(1 + z_{spec})] \qquad (1)$$

where $\delta z = z_{spec} - z_{phot}$. Second, we report the normalized median absolute deviation (NMAD; Ilbert et al. 2009; Dahlen et al. 2013; Molino et al. 2017), given as

$$\sigma_{NMAD} = 1.48 \times \mathrm{median}\left(\frac{|\delta z|}{1 + z_{spec}}\right). \qquad (2)$$

which provides an estimate of the scatter resistant to catastrophic outliers. Finally, the catastrophic outlier fraction (OLF) where we define a catastrophic outlier (following Molino et al. 2017) as,

$$\eta = \frac{|\delta z|}{(1 + z_{spec})} > 5 \times \sigma_{NMAD}. \qquad (3)$$

Figure 1 shows the photometric redshift performance as a function of the true spectroscopic redshift. For the full sample of galaxies we calculate $\sigma_f = XX\%$, $\sigma_{NMAD} = XX\%$, and an outlier fraction, $\eta = XX\%$. When considering the performance of only the galaxies se-
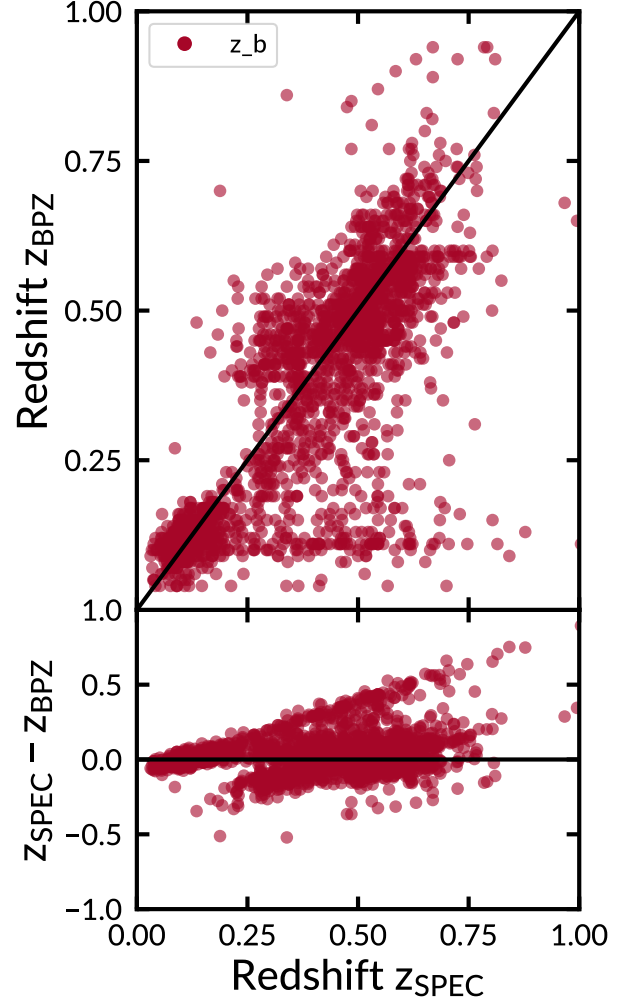

FIG. 1.— Comparison between photometric and spectroscopic redshifts for 2253 galaxies which have spectroscopic redshifts from the SDSS. The photometric redshifts in the top panel use a Bayesian approach with a custom empirical prior on galaxy brightness for the photometric redshifts. The bottom panel shows the difference between the spectroscopic and photometric redshift.

BPZ classified as E and E/S0 type, we find the following results; $\sigma_f = 10.4\%$, $\sigma_{NMAD} = 5.43\%$, and an outlier fraction, $\eta = 2.97\%$.

4.3. *Cluster Finding*

In this section, we briefly describe the algorithms and methods use to select the galaxy clusters from the multiwavelength optical/NIR imaging. We follow the methods described in detail in Menanteau et al. (2009, 2010a). We direct the reader there for an in depth description and discussion of the methods.

We first create a three-color image using STIFF (Bertin & Emmanuel 2011). The red, green, and blue channels are given by the corresponding combined mosaics described in Section 3.1. We then visually inspect an area of roughly $8' \times 8'$ centered on the position of each unconfirmed cluster; see Table 1. Potential brightest cluster galaxies (BCGs) are identified by first calculating the absolute limiting magnitude needs details.

Once a potential BCG is selected, the algorithm se-

lects nearby galaxies, within $|z_{BCG} - z| < 0.05$ and 0.5 Mpc projected radius, which BPZ has classified as either E or E/S0 galaxies. These photo-z's of the galaxies are combined using a 3σ median sigma-clipping algorithm to estimate the cluster's mean redshift, z_c. We use this mean cluster redshift measurement and the member selection criteria given previously to estimate the number of cluster members within 1 Mpc, N_{1Mpc}, which we define as the richness of the cluster, N_{gal}.

We correct the N_{gal} estimate by subtracting a statistical background of galaxies. We first estimate the number of background ellipticals by selecting galaxies within an annulus ($R_{200} < r < 2R_{200}$) around each cluster's position. We include galaxies with $\delta z = 0.05$ and similar colors as those galaxies assumed to belong to the cluster. These galaxies are subtracted from the cluster's population which provides an corrected N_{gal}, N_{galc}, which we then use to compute other important quantities. In practice the corrected number of galaxies is between 15% and 20% lower than the uncorrected number (Menanteau et al. 2010a). We report N_{galc} for the remainder of this work.

4.4. *Recovery of the Brightest Cluster Galaxies*

We have designed our observations to detect BCGs to $z \sim 1.5$. To quantify the actual depth of our images, we perform a Monte Carlo simulation by injecting artificial sources and computing their recovery fraction. We create the artificial sources with the MODELING package, part of ASTROPY (The Astropy Collaboration et al. 2013).

Following the procedure given in Menanteau et al. (2010b), the synthetic galaxies are created to have de Vaucouleurs (de Vaucouleurs 1948) profiles and surface brightnesses corresponding to their magnitude and assumed sizes. We inject the artificial galaxies into our science images with similar noise characteristics as their real counterparts.

We generate four rounds of one hundred elliptical galaxies spread uniformly across our science imaging. Each round of galaxies are place at different random positions to suppress abnormally boosted recovery fractions

due to source confusion. The artificial galaxies have total fluxes corresponding to apparent magnitudes between 19 mag $< i <$ 27 mag with 0.1 mag spacing. This is almost directly taken from FM2010 – edit. We use the individual field's completion limit to estimate the redshift to which we can reliably detect massive clusters. For this, we compare the completeness limits of our observations to the expected and observed (i.e., known) apparent magnitudes of galaxies in clusters as a function of redshift. We estimated the expected apparent galaxy i-band magnitude as a function of redshift using $L_\star$ as defined for the population of red galaxies by Blanton et al. (2003) at $z = 0.1$ and allowing passive evolution according to a solar metallicity (Bruzual & Charlot 2003) $\tau = 1.0$ Gyr burst model formed at $zf = 5$. We show this in Figure 3 for a range of luminosities ($L_\star$, $0.4L_\star$, and $4L_\star$) aimed at representing the cluster members from the faint ones to the BCG.

5. RESULTS

In this section we give the results of our visual cluster finding. During the inspection of each field, we classify each into four possible catalogs: High confidence, medium confidence, low confidence, and no detection. A high confidence result consists of a clear BCG and many accompanying satellite galaxies (see Figure **??**). A low confidence result is an ambiguous system where there is no clear BCG present but there appears to be a grouping of galaxies at a similar redshift. The medium confidence results fall in between the high and low confidence regimes where there appears to be a BCG but few satellite galaxies are observed. We fail to observe a cluster when there is no clear BCG candidate or clear group of galaxies at similar redshifts.

For the 112 fields observed with either MOSAIC or NEWFIRM, we observe twelve high confidence clusters, twenty two both medium and low confidence clusters, and we observe no discernible cluster in sixty fields. In the following subsections we present on each of the eight high confidence observations individually, and group the medium and low confidence observations together.

TABLE 2 Basic properties of the galaxy clusters candidates targeted for observation with the MOSAIC and NEWFIRM instruments: Column 1: Cluster name; Column 2: The right ascension of the cluster; Column 3: The declination of the cluster; Column 4: the PSZ catalog S/N ratio; Column 5: The date of MOSAIC observations; Column 6: The data of NEWFIRM observations.

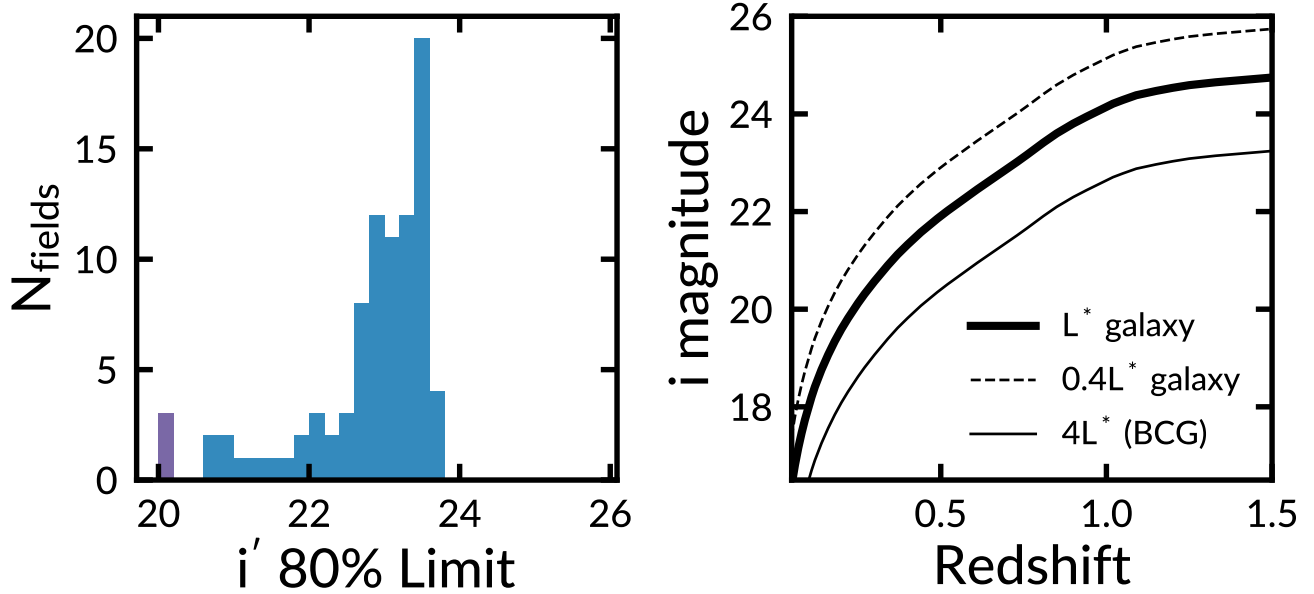| Cluster (1)	RA (J2000) (2)	DEC (J2000) (3)	PSZ1 SNR (4)	PSZ2 SNR (5)	MOSAIC Obs. (6)	NEWFIRM Obs. (7)
PSZ1 031.91+67.94	14:29:02	+24:37:33.38	5.23	nan	Feb, 2014	Feb, 2016
PSZ1 055.83-41.64	21:57:14	-2:31:51	5.72	nan	Oct, 2014	Nov, 2014
PSZ1 084.62-15.86	21:49:44	+33:10:23.81	6.01	nan	Oct, 2014	–
PSZ1 096.44-10.40	22:19:35	+44:31:05.27	6.55	nan	Oct, 2014	Nov, 2014
PSZ1 102.86-31.07	23:33:08	+28:43:51.60	6.12	nan	Oct, 2014	Nov, 2014
PSZ1 102.97-04.77	22:34:47	+52:43:13.90	5.64	nan	Oct, 2014	–
PSZ1 105.91-38.39	23:53:54	+22:34:21.09	7.16	nan	Oct, 2014	Nov, 2014
PSZ1 108.90-52.04	0:16:38	+09:52:49.98	6.89	nan	Jun, 2017	Nov, 2014
PSZ1 118.06+31.10	15:54:34	+84:10:37.49	6.00	nan	Feb, 2014	Mar, 2014
PSZ1 125.54-56.25	0:57:17	+06:35:23.29	4.86	nan	Nov, 2014	–
PSZ1 127.55+20.84	3:10:51	+82:25:43.91	5.91	nan	Oct, 2014	Nov, 2014
PSZ1 138.60-10.85	2:27:02	+49:04:54.07	8.26	nan	Oct, 2014	Nov, 2014
PSZ1 142.17+37.28	9:18:56	+70:52:01.14	5.79	nan	Feb, 2014	Mar, 2014
PSZ1 142.38+22.82	6:13:40	+71:52:21.02	5.82	nan	Feb, 2014	Mar, 2014
PSZ1 146.00-49.42	1:51:35	+10:44:02.79	6.62	nan	Oct, 2014	Nov, 2014
PSZ1 148.20+23.49	6:37:46	+66:54:24.40	8.40	nan	Feb, 2014	Mar, 2014
PSZ1 153.41+36.58	8:42:40	+62:34:31.61	6.85	nan	Feb, 2014	Mar, 2014
PSZ1 153.56+36.23	8:39:31	+62:31:30.58	5.96	nan	Feb, 2014	Mar, 2014

FIG. 2.— *Left:* Histogram of the *i*-band magnitude corresponding to 80% completeness in galaxy recovery. When 80% completeness is not achieved we show the limiting magnitude with the highest completeness. *Right:* Observed *i*-band magnitudes of $L_\star$, $0.4L_\star$, and $4L_\star$ (BCG) early-type galaxies as a function of redshift. We define an $L_\star$ galaxy following Blanton et al. (2003) as a population of red galaxies at $z = 0.1$ and allow it to evolve passively. The left and right panels can be combined to estimate the limiting redshift to which we could identify galaxy clusters.

TABLE 2 Continued

Cluster	RA (J2000)	DEC (J2000)	PSZ1 SNR	PSZ2 SNR	MOSAIC Obs.	NEWFIRM Obs.
(1)	(2)	(3)	(4)	(5)	(6)	(7)
PSZ1 162.30-26.92	3:24:26	+24:00:44.46	6.56	nan	Oct, 2014	Nov, 2014
PSZ1 169.80+26.10	7:30:08	+48:20:02.06	5.32	nan	Oct, 2014	–
PSZ1 182.49-57.09	2:44:20	-7:55:37	5.09	nan	Nov, 2014	–
PSZ1 183.26+12.25	6:42:56	+31:49:07.58	5.43	nan	Oct, 2014	–
PSZ1 185.93-31.21	4:11:39	+06:16:00.67	5.90	nan	Jan, 2014	Nov, 2014
PSZ1 206.45+13.89	7:29:59	+11:56:22.64	5.90	nan	Feb, 2014	Mar, 2014
PSZ1 224.82+13.62	8:01:42	-4:03:54	5.51	nan	Jan, 2014	–
PSZ1 244.48+34.06	9:49:52	-7:29:28	8.14	nan	Jan, 2014	Mar, 2014
PSZ1 249.01+73.75	11:56:46	+16:55:43.68	7.14	nan	Feb, 2014	Mar, 2014
PSZ1 286.25+62.68	12:21:10	+00:47:34.05	5.52	nan	Feb, 2014	Feb, 2016
PSZ1 341.69+50.66	14:25:20	-4:59:54	5.48	nan	Feb, 2014	–
PSZ2 022.03+17.75	17:28:37	-1:13:03	5.64	6.20	Jun, 2017	Feb, 2016
PSZ2 023.05+20.52	17:20:47	+00:58:06.58	nan	5.57	Jun, 2017	–
PSZ2 024.46-18.08	19:42:23	-15:26:09	nan	6.98	Jun, 2017	–
PSZ2 027.77+10.88	18:03:22	+00:25:57.59	nan	6.42	Jun, 2016	–
PSZ2 028.15-08.62	19:13:41	-8:08:26	5.07	7.67	Jun, 2017	–
PSZ2 029.66-47.63	21:45:44	-21:46:49	nan	5.74	Nov, 2016	–
PSZ2 029.80-17.40	19:48:32	-10:31:40	6.59	9.01	Jun, 2016	–
PSZ2 031.41-19.16	19:57:41	-9:53:56	4.60	5.69	Jun, 2017	–
PSZ2 032.12-14.96	19:43:34	-7:27:45	8.21	9.12	Jun, 2017	Nov, 2016
PSZ2 033.27-17.54	19:54:52	-7:36:11	5.78	6.86	Jun, 2017	–
PSZ2 036.69-15.67	19:54:05	-3:50:23	nan	5.69	Jun, 2017	–
PSZ2 043.44-41.27	21:36:44	-10:17:48	nan	5.55	Jun, 2017	–
PSZ2 044.83+10.02	18:36:39	+15:04:49.72	7.27	9.27	Oct, 2015	Feb, 2016
PSZ2 045.50-08.62	19:45:25	+07:04:29.08	4.57	5.63	Jun, 2017	–
PSZ2 047.53+08.55	18:46:59	+16:50:35.39	5.82	6.55	Jun, 2016	–
PSZ2 048.47+34.86	17:02:08	+27:08:48.05	nan	5.74	Jun, 2016	Feb, 2016
PSZ2 065.35-08.01	20:26:04	+24:08:06.72	nan	5.83	Jun, 2016	–
PSZ2 071.67-42.76	22:30:54	+05:42:05.22	8.82	8.63	Oct, 2014	Nov, 2014
PSZ2 075.08+19.83	18:46:48	+45:46:33.27	nan	5.74	Jun, 2016	–
PSZ2 089.06-11.79	21:52:53	+39:03:52.50	nan	5.72	Nov, 2016	–
PSZ2 092.11-33.73	23:01:37	+22:28:59.71	nan	5.81	Nov, 2016	Nov, 2016
PSZ2 092.46-35.22	23:05:50	+21:19:27.96	5.47	6.73	Oct, 2014	Nov, 2014
PSZ2 093.04-32.38	23:01:43	+24:02:24.90	5.69	6.03	Oct, 2014	Nov, 2014
PSZ2 096.43-20.89	22:48:09	+35:33:21.47	nan	5.81	Jun, 2016	Nov, 2016
PSZ2 098.38+77.22	13:18:25	+38:35:06.94	4.71	5.51	Jun, 2017	Nov, 2016
PSZ2 100.22+33.81	17:13:41	+69:22:24.33	nan	5.69	Jun, 2017	–
PSZ2 100.45+16.79	20:18:34	+66:47:07.85	nan	11.79	Oct, 2015	Nov, 2015
PSZ2 104.15-38.85	23:48:48	+21:43:24.60	nan	6.41	Jun, 2016	Nov, 2016
PSZ2 106.11+24.11	19:21:24	+74:33:21.87	nan	5.70	Jun, 2017	–

TABLE 2 Continued

Cluster	RA (J2000)	DEC (J2000)	PSZ1 SNR	PSZ2 SNR	MOSAIC Obs.	NEWFIRM Obs.
(1)	(2)	(3)	(4)	(5)	(6)	(7)
PSZ2 107.41-09.57	23:13:47	+50:19:32.01	nan	10.69	Jun, 2016	Nov, 2015
PSZ2 107.83-45.45	0:07:35	+16:07:51.05	nan	7.09	Nov, 2016	Nov, 2016
PSZ2 112.07-39.86	0:15:30	+22:14:43.50	nan	5.72	Nov, 2016	Nov, 2016
PSZ2 120.76+44.14	13:12:39	+72:53:23.47	nan	5.59	Jun, 2017	Feb, 2016
PSZ2 123.35+25.39	1:41:20	+88:13:14.57	5.90	10.86	Oct, 2014	Feb, 2016
PSZ2 123.84+25.75	2:55:30	+88:24:01.91	5.04	5.81	Nov, 2016	Feb, 2016
PSZ2 125.55+32.72	11:25:35	+83:57:29.12	nan	6.49	Nov, 2016	Feb, 2016
PSZ2 127.35-10.69	1:19:42	+51:56:15.39	5.58	6.94	Oct, 2014	Nov, 2014
PSZ2 136.31+54.67	11:47:50	+60:45:56.07	nan	6.92	Jun, 2017	Feb, 2016
PSZ2 137.24+53.93	11:41:07	+61:11:39.02	nan	7.87	Nov, 2016	Feb, 2016
PSZ2 137.58+53.88	11:39:27	+61:09:01.04	5.73	8.18	Feb, 2014	Mar, 2014
PSZ2 145.25+50.84	10:53:26	+60:51:43.24	nan	5.98	Jun, 2017	Feb, 2016
PSZ2 146.88+17.13	5:34:10	+65:43:14.28	nan	6.13	Nov, 2016	Feb, 2016
PSZ2 153.56+36.82	8:44:32	+62:24:41.96	nan	15.90	Nov, 2016	Nov, 2015
PSZ2 153.68+36.96	8:45:33	+62:17:12.13	nan	5.07	Nov, 2016	Nov, 2015
PSZ2 163.22-26.48	3:28:29	+23:50:15.15	nan	6.35	Nov, 2016	Feb, 2016
PSZ2 165.39+09.22	5:47:59	+46:08:39.24	nan	5.60	Nov, 2016	Nov, 2016
PSZ2 166.27-24.71	3:42:39	+23:24:41.39	nan	9.58	Nov, 2016	Nov, 2015
PSZ2 166.27-25.02	3:41:44	+23:11:00.45	nan	8.09	Nov, 2016	Nov, 2016
PSZ2 167.44-38.06	3:09:12	+12:37:11.49	6.11	7.66	Oct, 2014	–
PSZ2 171.79-42.08	3:08:40	+07:24:32.96	nan	5.84	Nov, 2016	Feb, 2016
PSZ2 173.76+22.92	7:17:28	+44:03:27.62	nan	5.80	Nov, 2016	Feb, 2016
PSZ2 181.88-30.77	4:04:21	+09:16:14.87	nan	9.29	Nov, 2016	Nov, 2015
PSZ2 185.45-32.01	4:08:04	+06:06:33.99	6.15	4.99	Jan, 2014	Nov, 2014
PSZ2 189.79-37.25	3:59:37	+00:07:54.80	6.99	7.28	Oct, 2014	Nov, 2014
PSZ2 191.82-26.64	4:38:37	+04:42:02.64	4.76	6.17	Nov, 2016	Feb, 2016
PSZ2 192.40-67.89	2:18:20	-17:45:23	nan	7.03	Nov, 2016	Feb, 2017
PSZ2 194.68-49.76	3:25:22	-9:40:50	5.00	5.71	Nov, 2016	Nov, 2016
PSZ2 210.37-37.00	4:32:44	-14:03:01	nan	9.84	Nov, 2016	Nov, 2015
PSZ2 210.71+63.08	10:51:42	+24:58:09.19	nan	7.37	Jun, 2017	Feb, 2016
PSZ2 210.78-36.25	4:36:07	-14:02:58	nan	6.32	Nov, 2016	Feb, 2016
PSZ2 252.45+73.44	11:58:35	+16:00:18.38	nan	5.57	Jun, 2017	Feb, 2016
PSZ2 305.76+44.79	12:59:54	-18:01:59	4.72	5.72	Jun, 2017	Feb, 2016
PSZ2 310.81+83.91	12:55:01	+21:05:41.16	nan	8.29	Nov, 2016	Feb, 2016
PSZ2 318.46+83.79	12:58:33	+21:08:11.93	6.93	9.40	Feb, 2014	Mar, 2014
PSZ2 320.94+83.69	12:59:47	+21:06:56.63	nan	7.32	Jun, 2017	Feb, 2016
PSZ2 328.96+71.97	13:23:13	+10:43:41.59	nan	5.85	Jun, 2017	Feb, 2016

Here are a few notes for the table.

5.1. *Observations of Known Clusters*

During the course of our observation campaign sixteen PSZ1 clusters were confirmed. We can use this opportunity to validate our cluster detection method against known clusters. The sixteen clusters are indicated in Table 2.

Thirty four of our fields were also observed by Barrena et al. (2018). Our results broadly agree with their findings.d We discuss individual differences in the notes on specific clusters below.

5.2. *High Confidence*

5.2.1. *PSZ1_G224.82+13.62*

5.2.2. *PSZ2_G029.66-47.63*

5.2.3. *PSZ2_G043.44-41.27*

5.2.4. *PSZ2_G096.43-20.89*

5.2.5. *PSZ2_G106.11+24.11*

5.2.6. *PSZ2_G120.76+44.14*

5.2.7. *PSZ2_G173.76+22.92*

5.2.8. *PSZ2_G305.76+44.79*

5.3. *Redshift Limits in Other Fields*

Lorem ipsum dolor amet swag copper mug meh tilde, put a bird on it live-edge tattooed kinfolk before they sold out locavore selvage leggings raclette literally bicycle rights. Hot chicken kickstarter mustache vinyl roof party. Wayfarers brooklyn truffaut twee umami, venmo irony. Typewriter viral pop-up, listicle vaporware organic af salvia keytar twee chillwave austin +1 offal blog. La croix dreamcatcher snackwave, try-hard intelligentsia taxidermy messenger bag air plant godard mustache celiac glossier echo park. Photo booth readymade authentic glossier biodiesel snackwave beard hammock sriracha before they sold out edison bulb fixie PBR&B. Man bun pabst kogi, crucifix subway tile af tacos cray tumeric lyft cronut lomo tattooed.

6. DISCUSSION

Lorem ipsum dolor amet swag copper mug meh tilde, put a bird on it live-edge tattooed kinfolk before they sold out locavore selvage leggings raclette literally bicycle rights. Hot chicken kickstarter mustache vinyl roof party. Wayfarers brooklyn truffaut twee umami, venmo irony. Typewriter viral pop-up, listicle vaporware organic af salvia keytar twee chillwave austin +1 offal blog. La croix dreamcatcher snackwave, try-hard intelligentsia taxidermy messenger bag air plant godard mustache celiac glossier echo park. Photo booth readymade authentic glossier biodiesel snackwave beard hammock sriracha before they sold out edison bulb fixie PBR&B. Man bun pabst kogi, crucifix subway tile af tacos cray tumeric lyft cronut lomo tattooed.

7. SUMMARY

Lorem ipsum dolor amet swag copper mug meh tilde, put a bird on it live-edge tattooed kinfolk before they

sold out locavore selvage leggings raclette literally bicycle rights. Hot chicken kickstarter mustache vinyl roof party. Wayfarers brooklyn truffaut twee umami, venmo irony. Typewriter viral pop-up, listicle vaporware organic af salvia keytar twee chillwave austin +1 offal blog. La croix dreamcatcher snackwave, try-hard intelligentsia taxidermy messenger bag air plant godard mustache celiac glossier echo park. Photo booth readymade authentic glossier biodiesel snackwave beard hammock sriracha before they sold out edison bulb fixie PBR&B. Man bun pabst kogi, crucifix subway tile af tacos cray tumeric lyft cronut lomo tattooed.

ACKNOWLEDGEMENTS

REFERENCES

Alam, S., Albareti, F. D., Prieto, C. A., et al. 2015, The Astrophysical Journal Supplement Series, 219, 12
Barrena, R., Streblyanska, A., Ferragamo, A., et al. 2018, eprint arXiv:1803.05764, arXiv:1803.05764
Benitez, N. 2000, The Astrophysical Journal, 536, 571
Bertin, E. 2006, in Astronomical Society of the Pacific Conference Series, Vol. 351, Astronomical Data Analysis Software and Systems XV, ed. C. Gabriel, C. Arviset, D. Ponz, & S. Enrique, 112
Bertin, E., & Arnouts, S. 1996, Astronomy and Astrophysics Supplement Series, 117, 393
Bertin, E., & Emmanuel. 2011, Astrophysics Source Code Library, record ascl:1110.006
Bertin, E., Mellier, Y., Radovich, M., et al. 2002, in Astronomical Society of the Pacific Conference Series, Vol. 281, Astronomical Data Analysis Software and Systems XI, ed. D. Bohlender, D. Durand, & T. Handley, 228
Blanton, M. R., Hogg, D. W., Bahcall, N. A., et al. 2003, The Astrophysical Journal, 592, 819
Bruzual, G., & Charlot, S. 2003, Monthly Notices of the Royal Astronomical Society, 344, 1000
Carlstrom, J. E., Ade, P. A. R., Aird, K. A., et al. 2011, Publications of the Astronomical Society of the Pacific, 123, 568
Chabrier, G. 2003, Publications of the Astronomical Society of the Pacific, 115, 763
Chambers, K. C., Magnier, E. A., Metcalfe, N., et al. 2016, eprint arXiv:1612.05560, arXiv:1612.05560
Coe, D., Benitez, N., Sanchez, S. F., et al. 2006, The Astronomical Journal, 132, 926
Dahlen, T., Mobasher, B., Faber, S. M., et al. 2013, The Astrophysical Journal, 775, 93
De Propris, R., Stanford, S. A., Eisenhardt, P. R., Dickinson, M. E., & Elston, R. 1999, The Astronomical Journal, Volume 118, Issue 2, pp. 719-729., 118, 719
de Vaucouleurs, G. 1948, Annales d'Astrophysique, 11, 247
Flewelling, H. A., Magnier, E. A., Chambers, K. C., et al. 2016, eprint arXiv:1612.05243, arXiv:1612.05243
Foley, R. J., Andersson, K., Bazin, G., et al. 2011, The Astrophysical Journal, 731, 86
Gaia Collaboration, G., Brown, A. G. A., Vallenari, A., et al. 2016a, Astronomy & Astrophysics, Volume 595, id.A2, 23 pp., 595, arXiv:1609.04172
Gaia Collaboration, G., Prusti, T., de Bruijne, J. H. J., et al. 2016b, Astronomy & Astrophysics, Volume 595, id.A1, 36 pp., 595, arXiv:1609.04153
Hunter, J. D. 2007, Computing in Science & Engineering, 9, 90
Ilbert, O., Capak, P., Salvato, M., et al. 2009, The Astrophysical Journal, 690, 1236
Jenkins, A., Frenk, C. S., White, S. D. M., et al. 2001, Monthly Notices of the Royal Astronomical Society, 321, 372
Komatsu, E., Smith, K. M., Dunkley, J., et al. 2011, The Astrophysical Journal Supplement Series, 192, 18
Menanteau, F., Hughes, J. P., Jimenez, R., et al. 2009, The Astrophysical Journal, 698, 1221
Menanteau, F., Hughes, J. P., Barrientos, L. F., et al. 2010a, The Astrophysical Journal Supplement Series, 191, 340
Menanteau, F., González, J., Juin, J.-B., et al. 2010b, The Astrophysical Journal, 723, 1523
Menanteau, F., Hughes, J. P., Sif?n, C., et al. 2012, The Astrophysical Journal, 748, 7
Molino, A., Benítez, N., Ascaso, B., et al. 2017, Monthly Notices of the Royal Astronomical Society, 470, 95
Mommert, M., & M. 2017, Astronomy and Computing, 18, 47
Ochsenbein, F., Bauer, P., & Marcout, J. 2000, Astronomy and Astrophysics Supplement Series, 143, 23
Oke, J. B. 1974, The Astrophysical Journal Supplement Series, 27, 21
Perez, F., & Granger, B. E. 2007, Computing in Science & Engineering, 9, 21
Planck Collaboration, Ade, P. A. R., Aghanim, N., et al. 2014, Astronomy & Astrophysics, 571, A29
—. 2016, Astronomy & Astrophysics, 594, A27
Probst, R. G., Gaughan, N., Abraham, M., et al. 2004, in Ground-based Instrumentation for Astronomy. Edited by Alan F. M. Moorwood and Iye Masanori. Proceedings of the SPIE, Volume 5492, pp. 1716-1724 (2004)., Vol. 5492, 1716
Skrutskie, M. F., Cutri, R. M., Stiening, R., et al. 2006, The Astronomical Journal, 131, 1163
Sunyaev, R. A., & Zeldovich, Y. B. 1972, Comments on Astrophysics and Space Physics, 4
Swaters, R. A., Valdes, F., & Dickinson, M. E. 2009, in Astronomical Society of the Pacific Conference Series, Vol. 411, Astronomical Data Analysis Software and Systems XVIII, ed. D. Bohlender, D. Durand, & P. Dowler, 506
Swetz, D. S., Ade, P. A. R., Amiri, M., et al. 2011, The Astrophysical Journal Supplement Series, 194, 41
The Astropy Collaboration, Robitaille, T. P., Tollerud, E. J., et al. 2013, Astronomy & Astrophysics, 558, A33
Tinker, J., Kravtsov, A. V., Klypin, A., et al. 2008, The Astrophysical Journal, 688, 709
Tody, D. 1993, Astronomical Data Analysis Software and Systems II, 52
Valdes, F. G., & Swaters, R. A. 2007, in Astronomical Society of the Pacific Conference Series, Vol. 376, Astronomical Data Analysis Software and Systems XVI, ed. R. Shaw, F. Hill, & D. Bell, 273

York, D. G., Adelman, J., Anderson, John E., J., et al. 2000, The
    Astronomical Journal, 120, 1579